Destruction of Raman biosignatures by ionising radiation and the implications for life detection on Mars

Lewis R. Dartnell, Kristian Page, Susana E. Jorge-Villar, Gary Wright, Tasnim Munshi, Ian J. Scowen, John M. Ward & Howell G. M. Edwards

Analytical and Bioanalytical Chemistry

ISSN 1618-2642
Volume 403
Number 1

Anal Bioanal Chem (2012) 403:131-144
DOI 10.1007/s00216-012-5829-6

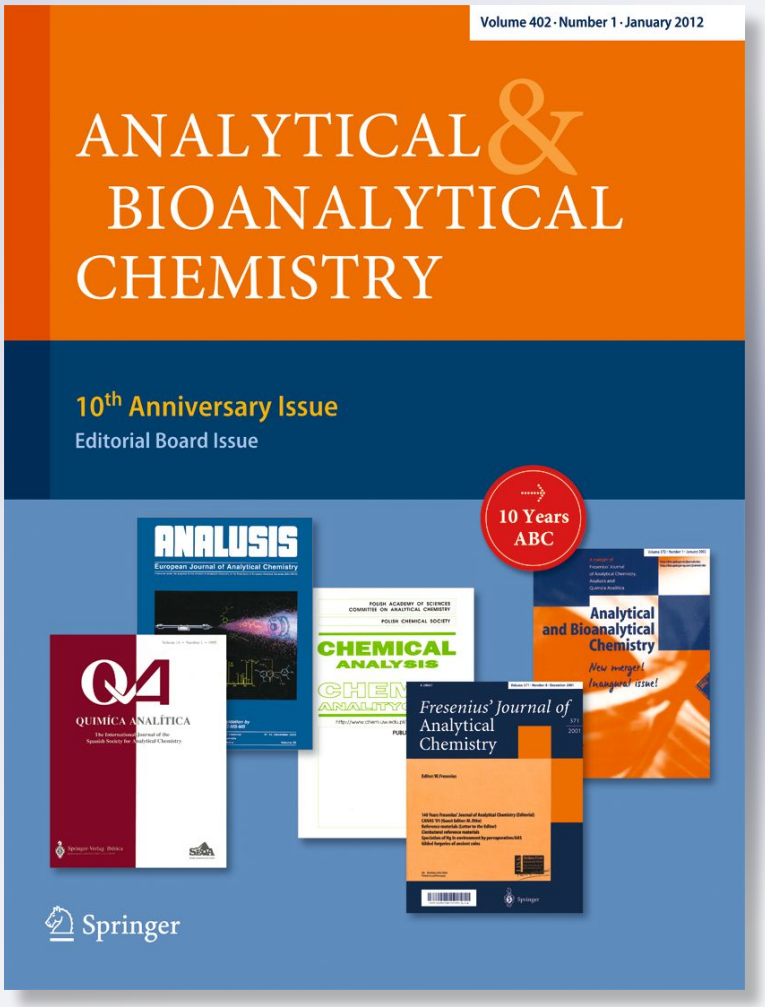

Springer

Anal Bioanal Chem (2012) 403:131–144
DOI 10.1007/s00216-012-5829-6

PAPER IN FOREFRONT

Destruction of Raman biosignatures by ionising radiation and the implications for life detection on Mars

Lewis R. Dartnell · Kristian Page · Susana E. Jorge-Villar · Gary Wright · Tasnim Munshi · Ian J. Scowen · John M. Ward · Howell G. M. Edwards

Received: 6 December 2011 / Revised: 1 February 2012 / Accepted: 1 February 2012 / Published online: 21 February 2012

Abstract Raman spectroscopy has proven to be a very effective approach for the detection of microorganisms colonising hostile environments on Earth. The ExoMars rover, due for launch in 2018, will carry a Raman laser spectrometer to analyse samples of the martian subsurface collected by the probe's 2-m drill in a search for similar biosignatures. The martian surface is unprotected from the flux of cosmic rays, an ionising radiation field that will degrade organic molecules and so diminish and distort the detectable Raman signature of potential martian microbial life. This study employs Raman spectroscopy to analyse samples of two model organisms, the cyanobacterium *Synechocystis* sp. PCC 6803 and the extremely radiation resistant polyextremophile *Deinococcus radiodurans*, that have been exposed to increasing doses of ionising radiation. The three most prominent peaks in the Raman spectra are from cellular carotenoids: deinoxanthin in *D. radiodurans* and β-carotene in *Synechocystis*. The degradative effect of ionising radiation is clearly seen, with significant diminishment of carotenoid spectral peak heights after 15 kGy and complete erasure of Raman biosignatures by 150 kGy of ionising radiation. The Raman signal of carotenoid in *D. radiodurans* diminishes more rapidly than that of *Synechocystis*, believed to be due to deinoxanthin acting as a superior scavenger of radiolytically produced reactive oxygen species, and so being destroyed more quickly than the less efficient antioxidant β-carotene. This study highlights the necessity for further experimental work on the manner and rate of degradation of Raman biosignatures by ionising radiation, as this is of prime importance for the successful detection of microbial life in the martian near subsurface.

L. R. Dartnell
UCL Institute for Origins, University College London,
Gower Street,
London WC1E 6B, UK

L. R. Dartnell (✉)
The Centre for Planetary Sciences at UCL/Birkbeck,
Earth Sciences, University College London,
Gower Street,
London WC1E 6B, UK
e-mail: l.dartnell@ucl.ac.uk

K. Page · T. Munshi · I. J. Scowen
Division of Chemical and Forensic Sciences,
University of Bradford,
Bradford BD7 1DP, UK

S. E. Jorge-Villar
Área de Geodinámica Interna,
Facultad de Humanidades y Educación,
C/ Villadiego s/n,
09001 Burgos, Spain

G. Wright
Department of Engineering and Applied Science,
Cranfield University,
Shrivenham, Swindon SN6 8LA, UK

J. M. Ward
Research Department of Structural and Molecular Biology,
University College London,
Gower Street,
London WC1E 6B, UK

H. G. M. Edwards
Centre for Astrobiology and Extremophiles Research,
School of Life Sciences, University of Bradford,
Bradford, West Yorkshire BD7 1DP, UK

Keywords Raman spectroscopy · Cosmic rays · Biosignature · Mars · Astrobiology · Microbe

Introduction

Raman spectroscopy of extremophilic microbes

Raman spectroscopy is an analytical technique based on inelastic scattering of laser excitation light able to reveal information on the vibrational and rotational modes within a target. For organic molecules, these Raman shifts relate primarily to vibrational modes and so are determined by the molecular structure, including bond types and functional groups. The Raman spectrum of a particular molecule represents a unique fingerprint of the bonds between its atoms and functional groups [1, 2] and with several corroborative bands the identification of molecular species can be precise [3].

Raman spectroscopy is also sensitive to mineralogy (see [1] and references therein). So, a Raman spectrum allows sensitive detection of microbial life colonising a sample as well as geochemical conditions of their microhabitat. The Raman spectrum between about 200 and 4,000 cm^{-1} includes most vibrational modes of both minerals and organic molecules, with mineral signals found mostly at low wavenumbers, and the bands from C–H bonds characteristic of organic compounds near 3,000 cm^{-1} [4].

Raman spectroscopy has thus proved to be a very effective technique for the in situ analysis of microbial communities in extreme environments on Earth, similar to extraterrestrial locations of interest to astrobiology, including the McMurdo Dry Valleys in Antarctica [4, 5], across an Antarctic transect [6], and within halite crusts in the hyperarid Atacama desert [7].

'Extremophilic' microorganisms in such hostile habitats produce characteristic compounds to aid survival and protect themselves from environmental stresses. These include photosynthetic pigments such as chlorophyll and accessory pigments including phycocyanin [4, 7], ultraviolet-screening compounds such as scytonemin [8] and β-carotene [1, 4] shown in Fig. 6, photoprotection and antioxidant molecules like carotenoids [1], and compounds involved in nutrient scavenging such as oxalate [4]. Many of these compounds degrade into recalcitrant well-preserved fossil biosignatures: chlorophyll degrades to porphyrins and carotenoids to isoprenoids and hopanoids, all of which contain moieties that produce characteristic Raman signatures [1, 9]. Although Raman spectroscopy has been used to infer a biological origin of carbonaceous residues as old as the early Archaen, abiotic processes have been shown to produce carbonaceous material similar to biogenic kerogen and Marshall et al. [10] caution against the interpretation of such ancient biosignatures until a suitable database of Raman spectral features from biogenic and abiogenic material has been constructed.

Raman spectroscopy in astrobiology

Laser Raman spectroscopy has been proposed as a promising technique for planetary exploration and the search for life beyond Earth by lander or rover (see [1–4, 6, 10, 11] and references within these). Raman spectroscopy presents many advantages over previous instrumentation deployed by robotic surface probes such as gas chromatography–mass spectrometry, including (list compiled from information in [1, 3]):

- Raman is sensitive to both organic and inorganic components of a heterogenous target system, thus allowing detection of biomolecules as well as their mineralogical context
- Sample preparation, either mechanical (i.e. powdering) or chemical (i.e. solvent extraction), is not necessary and so microbial communities can be studied undisturbed in their niche
- Raman is a non-destructive technique
- The nature of the specimen surface, such as irregular, fractured or polished, is not important
- Raman analysis is invariant to sample size, from microscopic to macroscopic targets
- Fibre-optic-based Raman spectrometers allow remote sensing of inaccessible targets such as subsurface boreholes

The ExoMars rover is an ESA mission [12], now likely to be merged with NASA involvement, designed specifically to look for signs of life on Mars and due for launch in 2018. The ExoMars confirmed scientific payload includes the Raman laser spectrometer (RLS) instrument; the first time a Raman spectrometer will be launched on a planetary mission. The ExoMars RLS will analyse crushed soil samples retrieved from the martian near subsurface by the rover's drill. RLS uses green excitation light at a wavelength of 532 nm, and the spectrometer unit offers a spectral range of 200–3,800 cm^{-1} (covering both mineralogical and biological signals), at a spectral resolution of 6–8 cm^{-1} [13].

A major hazard in the martian near subsurface that may act to degrade microbial biosignatures otherwise detectable by Raman spectroscopy, however, is the flux of cosmic radiation.

Cosmic rays

Beyond the shielding influence of Earth's magnetic field and atmosphere, the space environment is pervaded by an ionising radiation field known as cosmic rays, composed of

both solar energetic particles (SEP) and galactic cosmic rays (GCR) [14].

SEPs, primarily protons, are accelerated by flares and coronal mass ejections to energies typically of tens to hundreds of megaelectronvolts (MeV). The total fluence, peak flux, and energy spectra vary greatly between individual SEP events (see comparison by Mewaldt [15]), and events can last between a few hours and a week (reviewed by Vainio et al. [16]). The flux of these SEP is thus sporadic in nature and also dependent on the 11-year solar activity cycle, one half of the 22-year Hale cycle due to the periodic reversal of the Sun's magnetic field [17]. Over long irradiation durations, such as the cumulative SEP fluence onto the martian surface over millennia, however, time-averaged SEP spectra can be used (e.g. [18, 19]).

The peak flux of GCR particles, at around 500 MeV/nucleon, is three to four orders of magnitude lower than the averaged SEP flux at 10 MeV (e.g. [19]), but the power law tail of the CR spectra extends up to 10^{20} eV at extremely low fluxes. The GCR spectrum is composed of 85% protons, 14% alpha (helium nuclei), and a small fraction of heavy ions (fully ionised atomic nuclei) and electrons (see [16, 20, 21] for discussion of the particle acceleration mechanism). GCR below about 1 GeV/nucleon are modulated by the heliosphere so their flux is anticorrelated with the solar activity cycle [22].

Thus, GCR and SEP represent two complementary populations of ionizing particles in space: GCR are present at a relatively constant low flux, but their spectra extend to very high energy levels, whereas SEP have a much higher flux at lower energies and are accelerated within sporadic events.

When an energetic cosmic ray primary particle strikes shielding matter, such as in the Earth's upper atmosphere, it produces extensive showers of secondary particles including nuclear fragments and gamma rays [23]. The flux of secondaries builds with increasing shielding depth until it reaches a peak, known as the Pfotzer maximum, after which the average particle energy is below the threshold for new particle production and the cascade is steadily absorbed. In Earth's atmosphere, the Pfotzer maximum occurs at the altitude of 15–26 km, depending on latitude and solar activity level [24].

The surface of Mars today receives negligible shielding against cosmic rays, due to its thin atmospheric column and lack of global dipolar magnetic field. These extensive cascades of secondary particles occur in the near subsurface, with the Pfotzer maximum lying in the top metre, although the precise depth of penetration is dependent on the density and composition of the surface shielding material (e.g. [25, 26]).

Ionising radiation is a major threat to the survival of microbial life, the persistence of detectable biosignatures, and the operation of spacecraft equipment and biosignature detection instrumentation (see review in Dartnell [27]). Cosmic radiation destroys biological molecules through ionization and radiolysis [28]. Thus, the cosmic rays represent a dominant hazard in the martian near-subsurface environment [25, 26, 29] and far exceed the penetration of the unfiltered solar UV flux. The ExoMars drill will be able to retrieve subsurface samples from a maximum depth of 2 m, and so cosmic radiation is a prime consideration within this accessible region. Furthermore, the photosynthetic lifestyle of cyanobacteria requires that they reside near the surface for access to sunlight, and thus on Mars such organisms, as well as their Raman-detectable remnant biosignatures, would be exposed to cosmic irradiation.

So, a major unresolved issue in the search for biosignatures of past or present microbial life on the martian surface is the effect of such long-duration irradiation on their preservation. How is the distinctive Raman fingerprint of different extremophile compounds modified or distorted by radiation-induced breakdown of these organic biosignatures, and at what rate are the Raman peaks diminished by exposure to ionising radiation?

This initial study on the issue uses ionizing radiation exposure experiments on the detectable Raman biosignatures of the model cyanobacterium *Synechocystis* sp. PCC 6803 and the extremely radiation resistant *Deinococcus radiodurans*.

Materials and methods

Cell culture preparation

Synechocystis sp. PCC 6803 was cultured to high cell density in 100 ml BG11 liquid growth medium [30] with a photon flux of 46 μE/m^2/s in a photosynthesis incubator (Innova 4340, New Brunswick Scientific, St. Albans, UK) at 25 °C with constant agitation of 130 rpm for 8 days. *Deinococcus* was cultured to high cell density in tryptone digest, glucose, and yeast extract liquid medium, composed as described in Ref. [31] and incubated for 8 days at room temperature with constant agitation on a vertical rotator at 40 rpm. The liquid cultures of both organisms were centrifuged at 15,000×*g* for 10 min (Eppendorf centrifuge 5804R) and the supernatant discarded. Seven millilitres of sterile phosphate-buffered solution (PBS; Dulbecco's phosphate-buffered solution, Sigma) was pipetted onto each pellet and vortexed briefly to resuspend the cells. This protocol was followed to produce high densities of cells in the PBS suspensions, but the exact density of colony forming units was not quantified.

For both the *Synechocystis* and *Deinococcus* concentrated cell suspensions, one millilitre samples were pipetted into 2.0 ml borosilicate clear glass vials (2-CV, Chromacol, purchased through Fisher Scientific) and stoppered with

screw-caps. All vials and caps had previously been sterilised by autoclaving. These samples were stored overnight refrigerated at 4 °C and transported to and from the irradiation facility chilled on ice.

Irradiation protocol

The ionising radiation exposures were carried out at the cobalt-60 radionuclide gamma-ray source at Cranfield University, Shrivenham, UK. Distance from the cylindrical source determines the dose rate of the sample irradiation, so the sample vials were positioned at an appropriate distance to yield the desired total dose after an exposure of 5 h. One set of samples were positioned to receive a total irradiation of 15 kGy, a second set were positioned within the source cylinder to receive 150 kGy, and a third set were designated as controls and remained unexposed. The accuracy of doses delivered to samples is ±5%, which includes error in the timing of the exposure, positioning of the sample, and dosimetry. Control samples (0 kGy exposure) were prepared and transported alongside the irradiation vials, but stored for the duration of the exposure outside the irradiation room. See Dartnell et al. [32] or Dartnell et al. [33] for further details on the irradiation protocol.

After irradiation, the exposed and control samples were split; half analysed with a 532-nm excitation Raman spectrometer and half with a 633-nm Raman, as explained below.

Five hundred thirty-two-nanometre Raman analysis

A Bruker Senterra micro-Raman spectrometer with an objective of ×40 magnification was used for the analysis at 532 nm. The laser power was 2 mW, to avoid sample damage through heat biomolecular degradation. Previous experimentation had confirmed that no molecular alteration was produced at this laser power. A spectral range between 200 and 1,800 cm^{-1} was recorded. Spot size on the sample was around 1 μm. Spectra were achieved at 10-s exposure time, and 40 accumulations were performed for improving signal-to-noise-ratio. The analyses were carried out directly on samples dried onto glass slides and repeated in five different spots for comparing spectra.

The uncorrected Raman spectra generated for both *Deinococcus* and *Synechocystis* samples showed a gradual slope up to higher wavenumbers and so a simple linear function was fitted as a baseline and subtracted for the spectra shown in Figs. 1 and 2.

Six hundred thirty-three-nanometre Raman analysis

Raman spectroscopic analysis was performed at the University of Bradford using a Renishaw RIAS instrument equipped with a diode laser emitting at 633 nm with the maximal output power of the diode laser at the source of 500 and ~50 mW at the sample. The instrument used a CCD detector and a diffraction grating (1,000 lines/mm) limiting the spectral range to ~2,100–100 cm^{-1} with a spectral resolution of 10 cm^{-1}. The instrument was attached to a fibre-optic probe with an objective lens. Calibration of the instrument is performed using the most intense peak within the silicon spectrum occurring at 520.0±0.10 cm^{-1}.

The samples were analysed by pipetting a small quantity of culture to fixed depth onto a polished metal slide that produced no Raman signal. All the samples were analysed using the ×5 optical objective, in order to maximise depth of field, and exposed to the laser for 10 s. The *Synechocystis* cyanobacterium samples were exposed to 1% of the laser power for one accumulation. The *Deinococcus* samples were exposed to 100% of the laser power and the spectra were averaged over 25 accumulations.

Background emission from the 633-nm Raman analysis of *Deinococcus* gave a humped distribution, so a sixth-order polynomial function (of the form: $a+bx+cx^2+dx^3+ex^4+fx^5+gx^6$) was fitted to this as a baseline and subtracted for the spectrum shown in Fig. 3.

Results

A total of 12 Raman spectroscopic analyses were performed: two microorganisms (*Deinococcus* and *Synechocystis* sp. PCC 6803) studied with two laser excitation wavelengths (532 and 633 nm) after exposure to three different doses of gamma rays (0 kGy, control; 15 kGy; and 150 kGy).

Figure 1 shows the Raman spectra of *D. radiodurans* between 1,700 and 300 cm^{-1}, using a laser excitation wavelength of 532 nm, and after exposure to 150 (top; black line) and 15 kGy (middle; dark grey line) of ionising radiation, compared against the unexposed control sample (bottom; pale grey line). The wavenumbers of the three most prominent peaks, located at 1,511, 1,152 and 1,003 cm^{-1}, are indicated. Also shown as faint horizontal lines are the baselines used in the calculation of the peak heights, used to quantify the degree of radiolytic destruction as plotted in Fig. 5.

Figure 2 displays the stacked Raman spectra of the *Synechocystis* cyanobacteria samples from 532-nm excitation, also colour coded from light to dark to indicate the radiation exposure. Background emission was more problematic for these cyanobacteria samples than the *Deinococcus*, and so the baseline-corrected spectra do not appear as flattened. The three most prominent peaks are also labelled, occurring at 1,518, 1,155 and 1,005 cm^{-1}, i.e. at slightly greater wavenumbers than the corresponding peaks detected in *D. radiodurans*.

The stacked Raman spectra collected for *D. radiodurans* excited at the slightly longer laser wavelength of 633 nm are

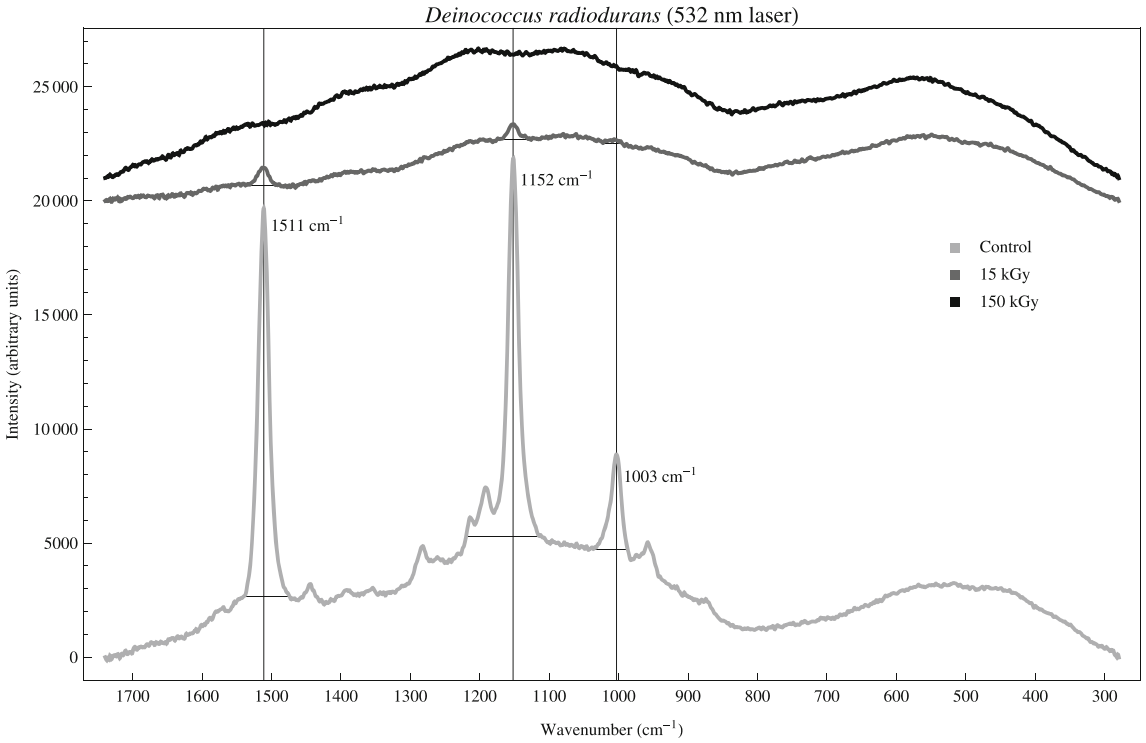

Fig. 1 Stacked Raman spectra (532-nm laser excitation) of *D. radiodurans* control sample and after exposure to 15 and 150 kGy of ionising radiation. Wavenumber of most prominent Raman peaks indicated

given in Fig. 3. The fitting function has proved very effective at yielding spectra with a flat baseline. The most salient peaks occur at 1,510, 1,152 and 1,003 cm^{-1}, noted to be essentially identical to those detected in the same organism with 532-nm

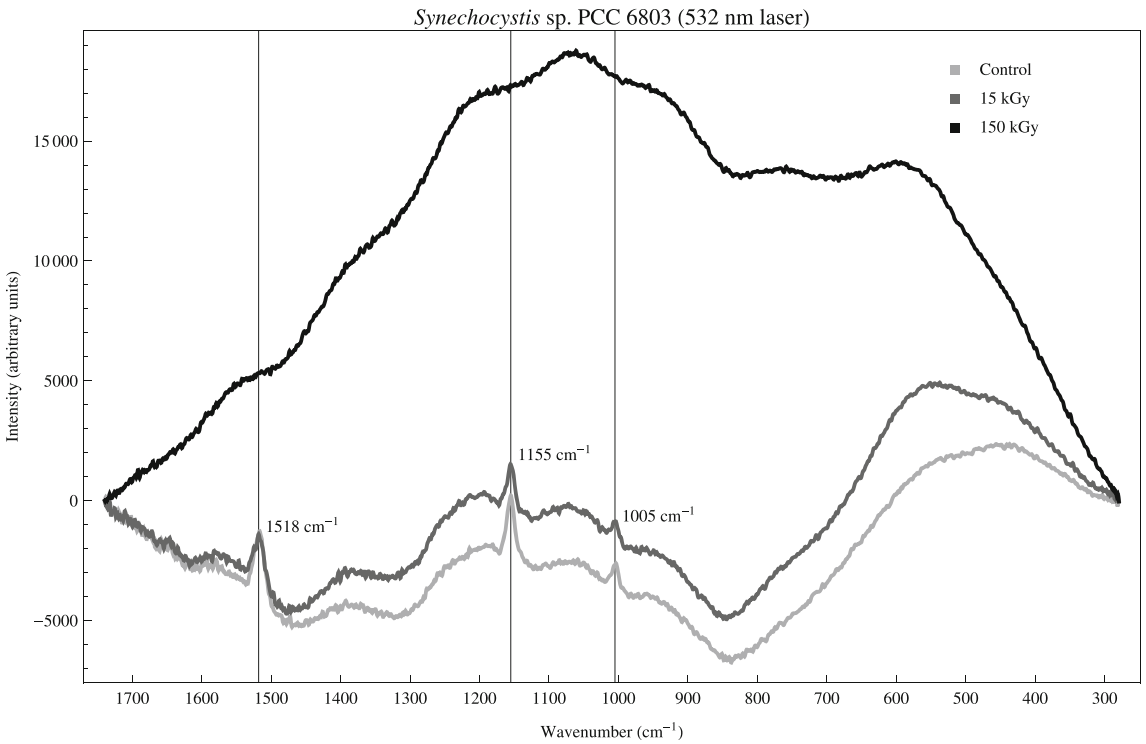

Fig. 2 Stacked Raman spectra (532-nm laser excitation) of *Synechocystis* control sample and after exposure to 15 and 150 kGy of ionising radiation. Wavenumber of most prominent Raman peaks indicated

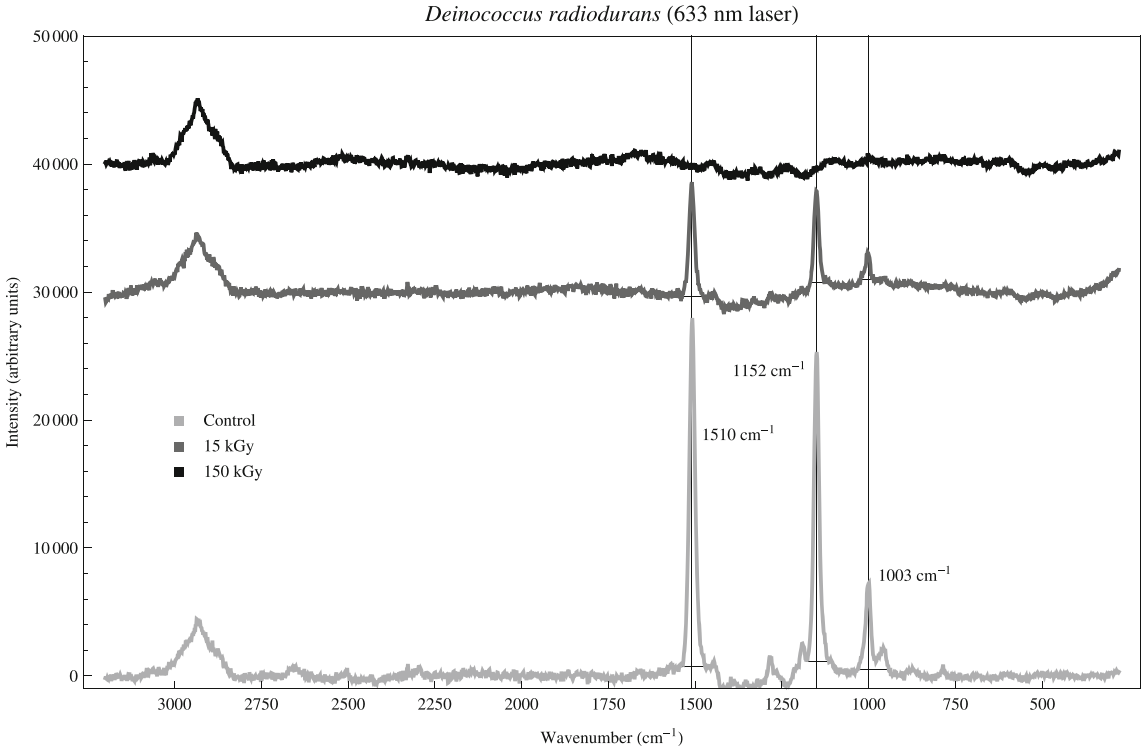

Fig. 3 Stacked Raman spectra (633-nm laser excitation) of *D. radiodurans* control sample, and after exposure to 15 and 150 kGy of ionising radiation. Wavenumber of most prominent Raman peaks indicated

excitation. A broader Raman feature is evident around 2,900 cm^{-1} and is seen to remain at a remarkably constant peak height between the unexposed control sample and maximum irradiation of 150 kGy. This 2,900 cm^{-1} spectral feature is not present in the blank slide analysis (spectrum not shown here) and so is a genuine signal from the cellular sample.

A comparison of the Raman spectra of the *Synechocystis* and *Deinococcus* samples after both have been exposed to the maximum dose of 150 kGy is shown in Fig. 4. It can be seen that despite the different nature of the two microorganisms, photosynthetic cyanobacterium and brightly pigmented polyextremophile, their Raman spectra are very similar after massive cellular degradation by the high radiation dose.

Figure 5 plots the change in Raman peak heights over increasing radiation exposure, as indicated in the spectra shown in Figs. 1, 2 and 3. Data are shown for each of the three prominent peaks in the spectra, measured by both 532- (green) and 633-nm (red) laser excitation for *D. radiodurans*, but only 532-nm laser excitation for the *Synechocystis* due to the domination of fluorescence background from the cyanobacterium at 633 nm.

Discussion

Results presented here show the Raman spectra of both the photosynthetic cyanobacterium *Synechocystis* sp. PCC 6803 and the brightly pigmented and extremely radiation resistant polyextremophile *D. radiodurans*. Analyses were performed with both 532- and 633-nm lasers, and results from *Deinococcus* are shown for both wavelengths, but no useful Raman spectra could be collected for *Synechocystis* with the 633-nm excitation. At this wavelength, any detectable Raman signal was swamped by excessive background emission from autofluorescence of the cyanobacterium's photosystem and other pigments. Dartnell et al. [34] characterise the complete fluorescent response (by generating fluorescence excitation-emission matrices) of several different model microorganisms including *Synechocystis* sp. PCC 6803 and *Deinococcus* (and see Dartnell et al. [33] for a closely related study on the rate of degradation of this cyanobacterial fluorescence biosignature by ionising radiation). The analysis shows that 633-nm light excites intense fluorescence from the cyanobacterial photosynthetic pigments phycocyanin and chlorophyl, whereas a wavelength of 532 nm induces much less fluorescence (of order five times less intense; Fig. 4 in Dartnell et al. [34]). *D. radiodurans*, a non-photosynthetic organism, exhibits negligible fluorescence at either 633 or 532 nm (Fig. 5 in Dartnell et al. [34]).

For the successful Raman analsyses, seen in Figs. 1 and 2 at 532-nm excitation and Fig. 3 at 633-nm excitation, both organisms exhibit three prominent Raman peaks at similar wavenumbers. These are identified as different vibrational and rocking modes of cellular carotenoid molecules.

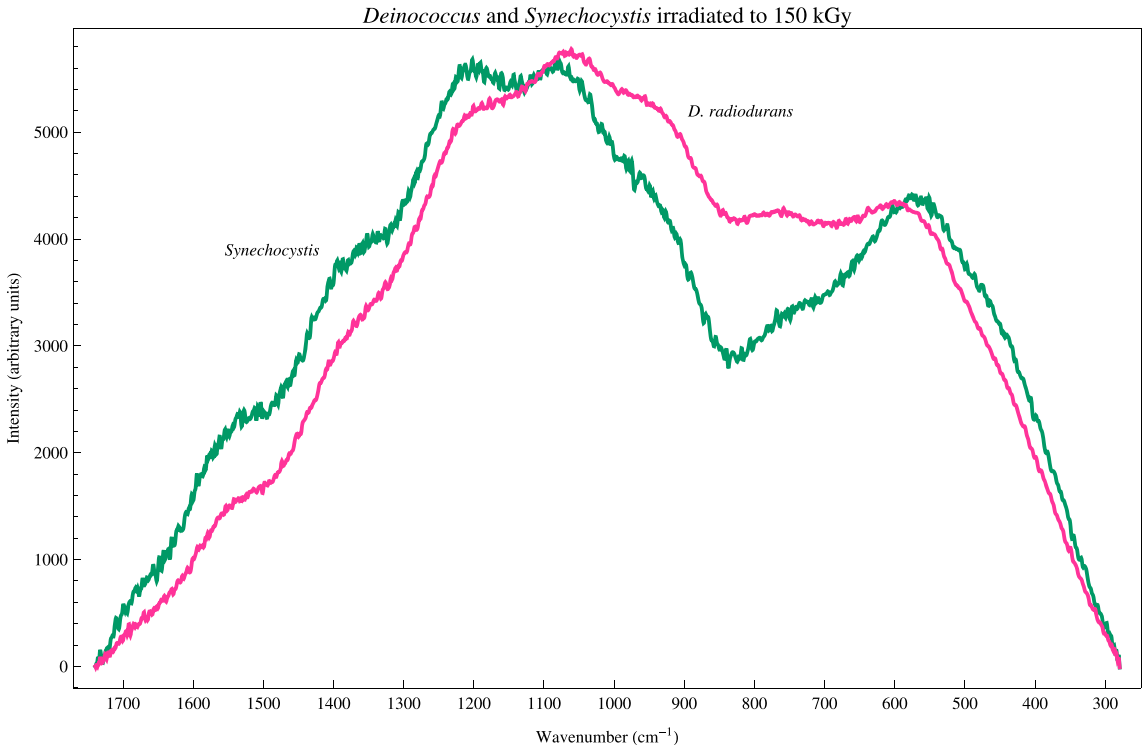

Fig. 4 Comparison of the Raman spectra produced by *Synechocystis* sp. PCC 6803 and *D. radiodurans* cells irradiated to the maximum dose of 150 kGy. The Raman spectra of these very different categories of microorganisms are remarkably similar after massive radiolytic cellular degradation

Cellular carotenoids

The carotenoids are a large class of lipid-soluble molecules, totalling around 600 distinct compounds. They are composed of a long π-electron-conjugated carbon-chain backbone, functionalised with groups such as hydroxy, keto, aldehyde and ester. Carotenoids are strongly coloured, due to an allowed π–π* electronic transition that falls within the visible spectrum, and range in appearance between dark red and pale yellow (indeed, the hues of autumnal leaves, and many fruit and vegetables are due to their carotenoid composition). Carotenoids are produced by all oxygenic photosynthetic bacteria (such as the *Synechocystis* species analysed here), as well as eukaryotic algae and higher plants, where they act as accessory pigments to increase the light-collection efficiency of the photosystems as well as acting to protect against photooxidation of the reaction centres. Carotenoids are also synthesised by non-photosynthetic bacteria (such as *D. radiodurans*) as they function as efficient scavengers of reactive oxygen species (ROS). This protective role of carotenoids will be discussed in depth later.

Carotenoids are promising biosignatures of microbial life surviving in extreme terrestrial habitats, as well as potentially on the martian surface, because they yield a distinctive fingerprint in the Raman spectrum. The identifications of the three prominent peaks seen in the spectra of *Deinococcus* and *Synechocystis* are listed in Table 1 (for assignment of these wavenumbers, see, for example, [6]). The Raman peak at around 1,515 cm^{-1} is due to vibrations about the carbon double bonds, ν_1(C=C), in the polyene chain of the carotenoid, whereas the peak at around 1,150 cm^{-1} is caused by a second vibrational mode, around carbon–carbon single bonds, ν_2(C–C). The spectral feature at around 1,000 cm^{-1} is from in-plane rocking modes of methyl groups attached to the polyene backbone coupled with C–C bonds.

Deinococcus analysed with both 532- and 633-nm lasers also shows smaller features in the spectral region 1,400–1,250 cm^{-1} due to in-plane rocking of C–CH and 1,000–700 cm^{-1} from out-of-plane wagging of hydrogen [35]. These less prominent spectral features were not included in the degradation rate analysis as they could not be reliably identified in the 15 kGy exposed samples.

Whilst *Synechocystis* excited at 532 nm shows a strong Raman signature of β-carotene, there were no detectable peaks from chlorophyll, expected at around 1,320 and 1,360 cm^{-1} from the tetrapyrrole ring [1, 3, 6]. However, Jorge-Villar and Edwards [3] note that the 1,326 cm^{-1} chlorophyll feature is detectable with 785-nm excitation but not with 514-nm excitation, due to the sensitivity of Raman scattering by pigments on the laser excitation wavelength. The Raman spectrum of *D. radiodurans* has been reported

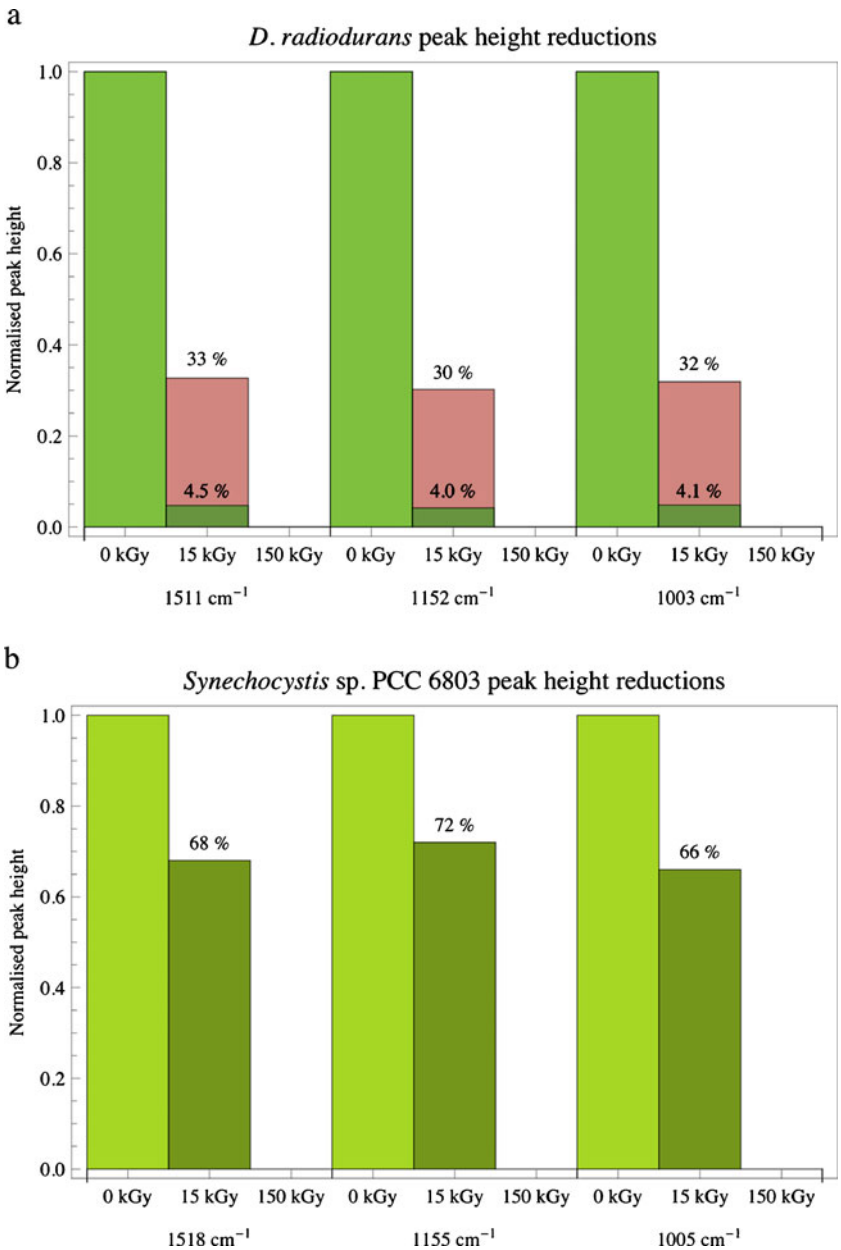

Fig. 5 The decrease in Raman spectral peak height measured for (**a**) *D. radiodurans* and (**b**) *Synechocystis* sp. PCC 6803 cells exposed to increasing doses of ionizing radaiation. Data from three prominent Raman peaks are shown at 1,511/1,518 cm^{-1} (*Deincococcus*/*Synechocystis*), 1,152/1,155 and 1,003/1,005 cm^{-1}. Colour coding indicates the excitation laser wavelength used 532 (*green*) and 633 nm (*red*), and the *darker shades* indicate the increasing radiation exposure. Only 532 nm (*green*) laser excitation yielded an analysable Raman spectrum for *Synechocystis*

by Edwards et al. [36] from 1,064-nm laser excitation, and here we supplement this with spectra generated from 532- and 633-nm excitation and find that the wavenumber of these carotenoid features agree very closely. Additionally, this current study is the first to examine the loss of signal from radiolytic degradation of biosignature molecules, as discussed further below.

Both *Deinococcus* and *Synechocystis* exhibit carotenoid peaks at very similar spectral locations, but importantly Table 1 shows that the ν_1(C=C) feature is found at a significantly lower wavenumber in *Deinococcus* (1,510 cm^{-1}) than the cyanobacterium (1,518 cm^{-1}). The location of the ν_1(C=C) Raman feature is strongly dependent on the number of C=C bonds in the polyene chain of the carotenoid

Table 1 Identification of the three prominent peaks in the Raman spectra shown in Figs. 1, 2 and 3, located at very similar wavenumbers in *Deinococcus radiodurans* and *Syncechocystis* sp. PCC 6803

Peak no.	*Deinococcus* wavenumber (cm^{-1})	*Syncechocystis* wavenumber (cm^{-1})	Compound	Mode
1	1,510	1,518	CAROTENOID	ν_1(C=C)
2	1,152	1,155	CAROTENOID	ν_2(C–C)
3	1,003	1,005	CAROTENOID	δ(C=CH)

molecule: the greater the number of conjugated bonds the lower the wavenumber of the corresponding ν_1(C=C) peak. The Raman spectra thus indicate that the primary carotenoid pigment synthesised by *Deinococcus* is a longer molecule than that of *Synechocystis*. Figure 6 shows the molecular structures of several representative carotenoids: both carotenes, hydrocarbons typically with backbones forty carbon atoms long (such as β-carotene), and xanthophylls, derivatives of carotenes that incorporate one or more oxygen atoms in functional groups (such as deinoxanthin).

High-performance liquid chromatography reveals that the brightly pigmented *Deinococcus* contains six coloured compounds with a β-carotene chromophore [37]. The dominant carotenoid synthesised by *D. radiodurans* has been named deinoxanthin [38], with a molecular structure determined as: (2R)-2,1′-dihydroxy-3′,4′-didehydro-1′,2′-dihydro-β, ψ-caroten-4-one [39], as shown in Fig. 6 (top). Deinoxanthin seems to be unique to the *Deinococcus* genus, although it is structurally similar to flexixanthin (a carotenoid produced by species of the *Flexibacter* genus [40]) as seen in Fig. 6. Both deinoxanthin and flexixanthin are believed to be synthesised from lycopene [41, 42], but deinoxanthin differs by an additional hydroxyl functional group on the C2 carbon of the β-ring [43]. In contrast to deinoxanthin, β-carotene is a very widespread pigment, and is the dominant carotenoid in *Synechocystis* cyanobacteria. Figure 6 shows β-carotene to possess only nine conjugate bonds in its structure, compared with 11 in the polyene backbone of deinoxanthin. It is this structural difference in the predominant carotenoid that explains the shift of the ν_1(C=C) feature in the *Deinococcus* and *Synechocystis* Raman spectra.

The colour of a carotenoid molecule also depends on the number of double bonds in the main carbon-chain: increasing the conjugation length yields hues passing from yellow through orange to deep red [44]. For example, β-carotene with its 11 conjugated bonds looks orange, bacterioruberin

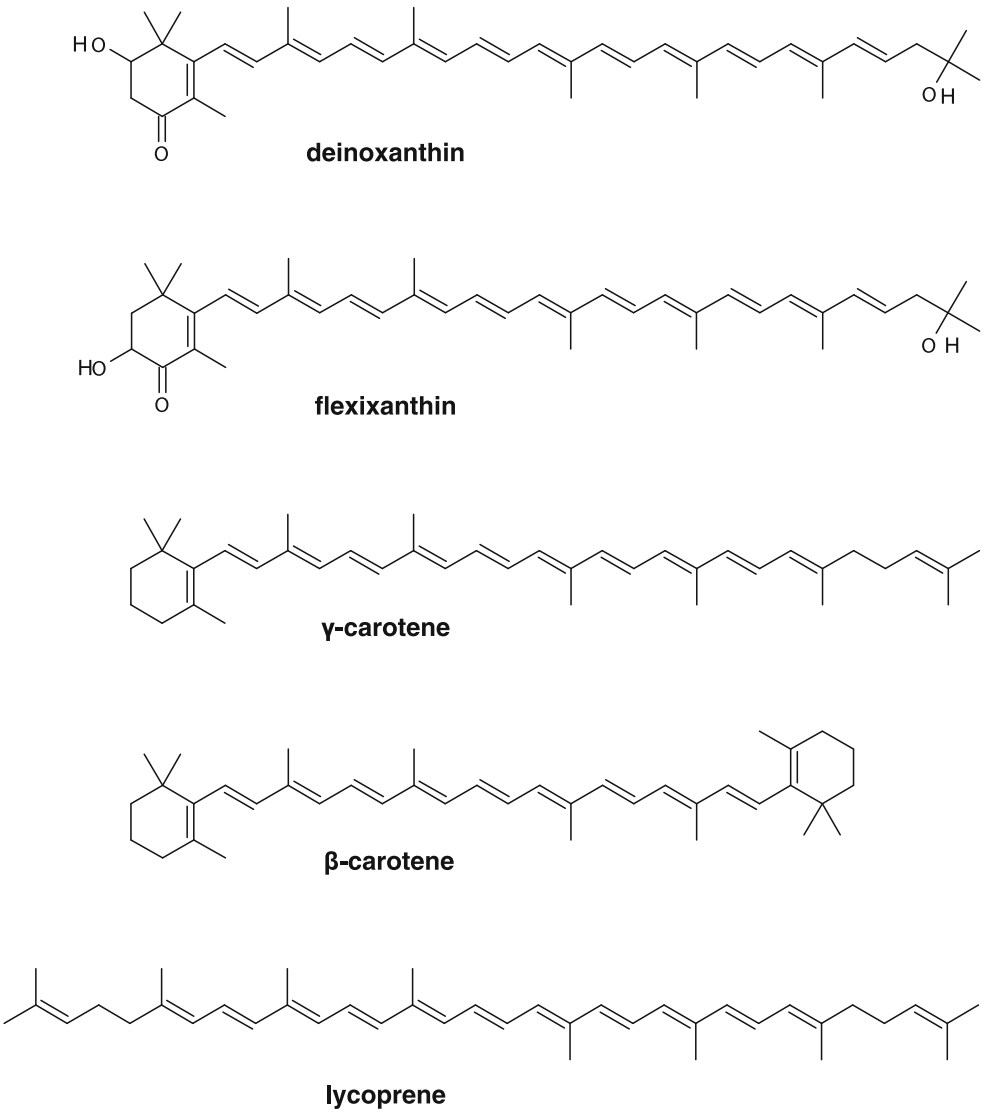

Fig. 6 Molecular structures of carotenoids relevant to this study: deinoxanthin, the C-2 hydroxyl monocyclic carotenoid unique to species of the *Deinococcus* genus [43]; flexixanthin, the structurally similar carotenoid produced by members of *Flexibacter* genus [40, 41]; γ- and β-carotene, common accessory pigments and antioxidants in both photosynthetic and nonphotosynthetic microorganisms; and lycopene, a carotene intermediate in the synthetic pathways for many carotenoids [49]

has 13 and appears a pinkish red [35] whereas *D. radiodurans* is a bright pink colour from deinoxanthin and its conjugation length of 12.

Rate of biosignature degradation

The central aim of this present study was to characterise the degradation of Raman biosignatures of the two representative microorganisms. *Synechocystis* sp. PCC 6803 is a model cyanobacterium that is easy to culture and has been well-characterised by genetic and photosynthetic research, and exhibits many of the same pigments and other cellular compounds as cyanobacteria living in extremophilic microhabitats. *Deinococcus* is a very radiation resistant microbe, and is often taken a model polyextremophile capable of tolerating martian conditions.

Figures 1, 2 and 3 show the Raman spectra generated for these two organisms after increasing exposure to ionising radiation, emulating the cosmic ray fluence on the martian surface. Substantial diminishment of the prominent spectral peaks is evident after 15 kGy of irradiation, and by 150 kGy the carotenoid biosignatures have been completely destroyed. Indeed, the Raman spectra of *Deinococcus* and *Synechocystis* samples exposed to the maximum irradiation (150 kGy) can be seen in Fig. 4 to be remarkably similar. These two distinct cell types, *Deinococcus* a very deeply rooted bacterium only closely phylogenetically related to the heat-tolerant *Thermus* genus [45] and with a unique carotenoid complement, and *Synechocystis* a photosynthetic cyanobacterium, appear to be very similar once their cellular biomolecules have been extensively degraded by radiation.

Figure 5 quantifies the rate of Raman signal loss, plotting the change in peak height for the three carotenoid features against radiation dose. Signal intensity of deinoxanthin carotenoid in *Deinococcus* from 633-nm excitation is reduced to one third after 15 kGy, and around 4% as measured by the 532-nm instrument. The detectable Raman signal from β-carotene in *Synechocystis* is down to about two thirds of the unirradiated control after 15 kGy. Whilst some variability in the rate of signal loss is apparent between 633- and 532-nm analyses of *D. radiodurans*, the three peaks measured in the same organism with the same wavelength are notably consistent with each other. It should also be stressed that the Raman signal strength from carotenoids is known to be closely dependent on the excitation wavelength used, and most notably when the laser wavelength coincides with an allowable π–π* electronic transition within the carotenoid the signal is greatly enhanced; the basis behind resonance Raman spectroscopy [35]. Regardless of this variation, the trend is very clear and by 150 kGy the Raman fingerprint of carotenoids in both *Synechocystis* and *Deinococcus* has been completely erased. By way of comparison, absorption spectroscopy of similarly irradiated *Synechocystis* sp. PCC 6803 cells implies that carotenoids have been completely degraded by 60 kGy of gamma rays [33].

These substantial reductions in the Raman biosignatures, particularly the complete absence of detectable signal after 150 kGy, are believed to be due to radiolytic destruction of the carotenoids by the high fluxes of ionising gamma-rays, and not inter-sample variability.

The broad Raman feature in the region of 2,900 cm^{-1} in the spectrum of *D. radiodurans* excited with 633-nm laser light (Fig. 3) is due to C–H stretching vibrational bands of aliphatic compounds [46]. Such a feature is indicative of aliphatic organic molecules, but not necessarily biological compounds in the way that carotenoids are an unambiguous biosignature. This 2,900 cm^{-1} feature is noted to be very stable in the face of high doses of ionising radiation, in contrast to the complete loss of signal from the three indicative peaks of the carotenoid. The standard error of the variation in the peak height of this feature is less than 6% across the three dose levels. Similarly, the broad background feature around 500 cm^{-1} in Figs. 1 and 2 from 532-nm excitation is also stable to the radiation exposure, with the standard error of variation being 7.5% across all three exposures of *Deinococcus* and 4.5% between the control and 15 kGy exposure of *Synechocystis*. The stark decreases in the peak heights of the labelled Raman biosignatures can thus be confidently ascribed to the molecular destruction of irradiation and not sample or measurement variation, and so the quantitative analysis shown in Fig. 5 is taken to be reliable.

Role of carotenoids in radiation resistance

In addition to demonstrating the total loss of detectable biosignatures after 150 kGy of ionising radiation, the results presented in Fig. 5 suggest that the carotenoid Raman fingerprint of the irradiated *Deinococcus* population is degraded more rapidly by the gamma ray flux than the carotenoids in the *Synechocystis* cyanobacterium. As seen in Fig. 6, the principal carotenoid in *Deinococcus*, deinoxanthin, is a longer chain molecule than the β-carotene in *Synechocystis*, and also contains one rather than two terminal ring structures. These structural features may render the carotenoid complement *Deinococcus* more susceptible to radiolytic break-down, by either the direct or indirect mechanisms, than that of the *Synechocystis* cells. Carotenoid molecules serve as accessory pigments to increase the efficiency of photosystems but are also synthesised by many non-photosynthetic bacteria as they function as efficient scavengers of ROS. As described in the Introduction, irradiation of water produces hydrated free electrons, free radicals such as the ·OH hydroxyl radical, and molecular oxidants like hydrogen peroxide, which diffuse from their site of production and attack biomolecules (see Dartnell [27] for a

summary of the reaction pathways of irradiated water). Carotenoids have an antioxidant function and can effectively scavenge these reactive oxygen species and free radicals [47, 48]. Carotenoids act as a non-enzymatic line of defence against oxidative stress (alongside enzymes such as superoxide dismutase and catalase that catalytically break-down ROS), sacrificially protecting a cell from the oxidizing products of radiation and so are themselves rapidly destroyed (see the excellent review of carotenoids presented in Armstrong [49], and references therein). Prior radiation exposure experiments reported by Dartnell et al. [33] have found that carotenoids diminish much more rapidly (as determined by absorption spectroscopy) than other cellular pigments such as chlorophyll and phycocyanin within irradiated cyanobacterial cells.

The prevalence of carotenoids in *Deinococcus* is thought to contribute to the organism's extreme radiation resistance, alongside enzymatic processes involved in ROS removal and DNA repair [50]. Tian et al. [43] demonstrated that deinoxanthin is particularly effective at scavenging both H_2O_2 and singlet oxygen, performing better than either carotenes (such as lycopene and β-carotene) or other xanthophylls (including zeaxanthin and litein). Targeted mutagenesis was used to knock-out the phyoene synthase gene and so block the carotenoid synthesis metabolic pathway. The mutants were thus unable to generate carotenoids, appearing unpigmented, and were found to be more sensitive to hydrogen peroxide, desiccation and ionising radiation than the wild type strain [43]. This complements earlier work showing that unpigmented *D. radiodurans* mutants are significantly more sensitive to oxidising hazards such as H_2O_2 and ionising radiation, as well as desiccation and UV radiation (e.g. [37, 51, 52]), although it is important to note that wildtype unpigmented members of the genus, such as *Deinococcus deserti*, can be as radioresistant as the intensely red *D. radiodurans* [53]. This may be partly due to the fact that some carotenoids, including phytoene, are colourless, and an apparently unpigmented strain may still synthesise some carotenoids [54] and so be afforded antioxidant protection.

The superior ROS-scavenging capability of deinoxanthin is believed to be due to its extended conjugated double bonds and hydroxyl functional end groups [54], as can be seen in Fig. 6. This enhanced scavenging ability of deinoxanthin, and the sacrificial protection against irradiation products it affords *D. radiodurans*, thus explains the more rapid degradation of the *Deinococcus* carotenoid signatures than the cyanobacterial Raman peaks that is evident in the plots in Fig. 5.

Necessity for further work

Many papers over recent years have stressed the applicability of Raman spectroscopy to planetary exploration, and in particular searching the martian surface for remnant biosignatures (see [1–4, 6, 10, 11] and references within these), but the response of target biosignature molecules to long-term exposure to cosmic radiation on Mars has not yet been addressed.

Previous studies have looked at the changes in Raman spectrum from organic material in a diagenetic series or exposed to ionising radiation. Marshall and Olcott Marshall [44] report the differences in Raman spectra between two biosignature carotenoids, β-carotene and lycopene (see Fig. 6), and their diagenetic products, the perhydro derivatives β-carotane and lycopane. These derivatives are formed by hydrogenation of the polyene chain and thus loss of all conjugated C=C bonds; the dominant chemical process during senescence and early diagenesis. They found, as would be expected, that the perhydro derivatives exhibit no Raman band around 1,512–1,518 cm^{-1} due to $\nu 1$(C=C) stretching (see Table 1) but instead show appearance of an intense band assigned to methylene scissoring and eight other bands due to variance vibrational modes of C–C bonds.

Court et al. [55] used Raman spectroscopy to analyse terrestrial organic matter (bitumens) that had been naturally irradiated in situ by the radionuclide content of their host rock. They found that whereas thermal maturation and metamorphism of organic matter generally leads to an increase in structural organisation, through carbonisation and graphitisation, the effects of long-term irradiation are to increase disorganisation.

This current study, however, is the first to examine the changes in the Raman spectra of microbial biosignatures with ionising radiation, which is a dominant environmental hazard on the martian surface. The radiolytic degradation of cellular compounds, or their refractory diagenetic products, by the long-term flux of cosmic rays will act to degrade biosignatures detectable by Raman spectroscopy and so frustrate life detection in the martian surface. This study has clearly demonstrated the significance of this effect and the erasure of Raman fingerprints of biosignatures by ionising radiation.

Further work is needed to study in greater detail this radiation-induced degradation of microbial biosignatures. This current study has found significant degradation by 15 kGy of ionising radiation, and total destruction of the Raman signal by 150 kGy, thus defining the limits for future work. On-going work will explore this defined range with greater dose resolution, and also explore the effect of temperature during irradiation. The martian near subsurface at midlattitudes varies between 230 and 180 K [56], and further irradiation experiments will examine to what extent a lower temperature limits the rate of degradation, as has been found, for example, on the effects of ionising radiation on organism survival [32, 57] and ultraviolet radiation on amino acid degradation [58].

We have found here a clear diminishment of Raman peak heights with irradiation, but another effect that might also be expected is a shift in the position of particular bands. For example, the wavenumber of the ν_1(C=C) band depends on the number of conjugate bonds in the carotenoid polyene backbone. If ionising radiation causes lysis of chains, or otherwise destroys C=C bonds, you might expect to see a shift or broadening of this spectral feature as carotenoids are steadily radiolysed to yield a population of fragments of different conjugate lengths.

The long-term flux of cosmic radiation is thus expected to not only diminish detectable Raman peak heights, but also potentially distort recognisable spectral fingerprints, and so to maximise the chance of success of astrobiological searches in the martian surface it is imperative to understand both the nature and rate of this biosignature degradation. Raman spectroscopy has also been proposed for biosignature detection in other astrobiological targets influenced by ionising radiation. For example, penetrator probes may investigate in situ the near-subsurface ice of Europa [59], an environment that is exposed to the very high flux of trapped particle radiation in the Jovian magnetic field. This question of the effects of ionising radiation on the detectability of Raman biosignatures is not therefore limited to the exploration of Mars.

This paper is intended as a clarion call for the necessary investigations into the effects of ionising radiation on the detectability of microbial biosignatures by Raman spectroscopy, in the crucial interests of astrobiology.

Conclusions

Raman spectroscopy is a promising technique for searching for biosignatures of microbial life in the surface and near subsurface of Mars. The model microbes *Synechocystis* sp. PCC 6803 and *D. radiodurans* have been shown here to yield a distinctive Raman biosignature. Three prominent peaks were observed in the Raman spectra of *D. radiodurans* from both 532- and 633-nm laser excitation, and of the *Synechocystis* cyanobacterium at 532 nm. These spectral features are identified as the ν_1(C=C) and ν_2(C–C) backbone vibrations and the δ(C=CH) rocking modes of cellular carotenoids: deinoxanthin in *D. radiodurans* and β-carotene in *Synechocystis*. The lower wavenumber of the ν_1(C=C) feature in *D. radiodurans* corresponds to the longer conjugate length of the polyene backbone of deinoxanthin. These distinctive biosignature Raman spectral features of carotenoids, common to photosynthetic and extremophilic microorganisms on Earth, thus represent a promising target for the RLS instrument aboard ExoMars. The unshielded flux of cosmic radiation onto Mars creates an ionizing radiation field that penetrates the top metres of the subsurface, and will act to degrade detectable organic biosignatures. This study has found a significant diminishment of Raman spectral peak heights after 15 kGy of ionising radiation, and complete erasure of Raman biosignatures by 150 kGy. The carotenoid signature of *Deinococcus* is observed to diminish more rapidly than that of *Synechocystis*. This is believed to be due to the fact that deinoxanthin is a superior scavenger of reactive oxygen species, such as produced by radiolysis, and so is destroyed more quickly than the less efficient antioxidant β-carotene. This present study highlights the necessity for further investigation into this effect of ionizing radiation, and the degradation rate of Raman biosignatures on Mars.

Acknowledgements LRD is supported by UCL Institute for Origins postdoctoral research associateship funding.

References

1. Ellery A, Wynn-Williams D (2003) Why Raman spectroscopy on Mars? A case of the right tool for the right job. Astrobiology 3:565–379
2. Tarcea N, Frosch T, Rösch P, Hilchenbach M, Stuffler T, Hofer S, Thiele H, Hochleitner R, Popp J (2008) Raman spectroscopy—a powerful tool for in situ planetary science. Space Sci Rev 135:281–292
3. Jorge Villar S, Edwards H (2006) Raman spectroscopy in astrobiology. Anal Bioanal Chem 384:100–113
4. Wynn-Williams D, Edwards H (2000) Proximal analysis of regolith habitats and protective biomolecules in situ by laser raman spectroscopy: overview of terrestrial antarctic habitats and mars analogs. Icarus 144:486–503
5. Jorge Villar S, Edwards H, Cockell C (2005) Raman spectroscopy of endoliths from Antarctic cold desert environments. Analyst 130:156–162
6. Edwards H, Moody C, Jorge Villar S, Wynn-Williams D (2005) Raman spectroscopic detection of key biomarkers of cyanobacteria and lichen symbiosis in extreme Antarctic habitats: evaluation for Mars Lander missions. Icarus 174:560–571
7. Vítek P, Edwards H, Jehlička J, Ascaso C, De Los RA, Valea S, Jorge-Villar S, Davila A, Wierzchos J (2010) Microbial colonization of halite from the hyper-arid Atacama Desert studied by Raman spectroscopy. Philos Transact A Math Phys Eng Sci 368:3205–3221
8. Cockell C, Knowland J (1999) Ultraviolet radiation screening compounds. Biol Rev Camb Philos Soc 74:311–145
9. Wynn-Williams DD, Edwards HGM (2000) Antarctic ecosystems as models for extraterrestrial surface habitats. Planet Space Sci 48:1065–1075
10. Marshall C, Edwards H, Jehlicka J (2010) Understanding the application of raman spectroscopy to the detection of traces of life. Astrobiology 10:229–240
11. Ellery A, Wynn-Williams D, Parnell J, Edwards HGM, Dickensheets D (2004) The role of Raman spectroscopy as an astrobiological tool in the exploration of Mars. J Raman Spectrosc 35:441–457
12. Vago J, Gardini B, Kminek G, Baglioni P, Gianfiglio G, Santovincenzo A, Bayon S, van Winnendael M (2006) ExoMars: searching for life on the red planet. ESA Bulletin, vol 126
13. Rull F, Sansano A, Diaz E, Canora C, Moral A, Tato C, Colombo M, Belenguer T, Fernandez M, Manfredi J, Canchal R, Davila B, Jimenez A, Gallego P, Ibarmia S, Prieto J, Santiago A, Pla J,

Ramos G, Gonzalez C (2010) ExoMars Raman laser spectrometer overview. Proc. SPIE, vol 7819

14. Amsler C, Doser M, Antonelli M, Asner D, Babu K, Baer H, Band H, Barnett R, Bergren E, Beringer J, Bernardi G, Bertl W, Bichsel H, Biebel O, Bloch P, Blucher E, Blusk S, Cahn R, Carena M, Caso C, Ceccucci A, Chakraborty D, Chen M, Chivukula R, Cowan G, Dahl O, D'Ambrosio G, Damour T, de Gouvêa A, DeGrand T, Dobrescu B, Drees M, Edwards D, Eidelman S, Elvira V, Erler J, Ezhela V, Feng J, Fetscher W, Fields B, Foster B, Gaisser T, Garren L, Gerber H, Gerbier G, Gherghetta T, Giudice G, Goodman M, Grab C, Gritsan A, Grivaz J, Groom D, Grünewald M, Gurtu A, Gutsche T, Haber H, Hagiwara K, Hagmann C, Hayes K, Hernández-Rey J, Hikasa K, Hinchliffe I, Höcker A, Huston J, Igo-Kemenes P, Jackson J, Johnson K, Junk T, Karlen D, Kayser B, Kirkby D, Klein S, Knowles I, Kolda C, Kowalewski R, Kreitz P, Krusche B, Kuyanov Y, Kwon Y, Lahav O, Langacker P, Liddle A, Ligeti Z, Lin C, Liss T, Littenberg L, Liu J, Lugovsky K, Lugovsky S, Mahlke H, Mangano M, Mannel T, Manohar A, Marciano W, Martin A, Masoni A, Milstead D, Miquel R, Mönig K, Murayama H, Nakamura K, Narain M, Nason P, Navas S, Nevski P, Nir Y, Olive K, Pape L, Patrignani C, Peacock J, Piepke A, Punzi G, Quadt A, Raby S, Raffelt G, Ratcliff B, Renk B, Richardson P, Roesler S, Rolli S, Romaniouk A, Rosenberg L, Rosner J, Sachrajda C, Sakai Y, Sarkar S, Sauli F, Schneider O, Scott D, Seligman W, Shaevitz M, Sjöstrand T, Smith J, Smoot G, Spanier S, Spieler H, Stahl A, Stanev T, Stone S, Sumiyoshi T, Tanabashi M, Terning J, Titov M, Tkachenko N, Törnqvist N, Tovey D, Trilling G, Trippe T, Valencia G, van Bibber K, Vincter M, Vogel P, Ward D, Watari T, Webber B, Weiglein G, Wells J, Whalley M, Wheeler A, Wohl C, Wolfenstein L, Womersley J, Woody C, Workman R, Yamamoto A, Yao W, Zenin O, Zhang J, Zhu R, Zyla P, Harper G, Lugovsky V, Schaffner P (2008) Cosmic rays. Physics Letters B 667:254–260
15. Mewaldt R (2006) Solar energetic particle composition, energy spectra, and space weather. Space Sci Rev 124:303–316
16. Vainio R, Desorgher L, Heynderickx D, Storini M, Flückiger E, Horne R, Kovaltsov G, Kudela K, Laurenza M, McKenna-Lawlor S, Rothkaehl H, Usoskin I (2009) Dynamics of the Earth's particle radiation environment. Space Sci Rev 147:187–231
17. O'Brien K (2007) Cosmic-ray propagation through the disturbed heliosphere. Acta Astronautica 60:541–546
18. Kuznetsov NV, Nymmik RA, Panasyuk MI (2001) The balance between fluxes of galactic cosmic rays and solar energetic particles, depending on solar activity. In: Proceedings of the 27th International Cosmic Ray Conference. Hamburg, Germany, vol 8
19. Usoskin IG, Kovaltsov GA (2006) Cosmic ray induced ionization in the atmosphere: full modeling and practical applications. J Geophys Res 111:D21206
20. Blandford R, Eichler D (1987) Particle acceleration at astrophysical shocks: A theory of cosmic ray origin. Physics Reports 154:1–75
21. Butt Y (2009) Beyond the myth of the supernova-remnant origin of cosmic rays. Nature 460:701–704
22. Klapdor-Kleingrothaus HV, Zuber K (2000) Chapter 8: cosmic radiation. Particle Astrophysics 223–247
23. Amsler C, Doser M, Antonelli M, Asner D, Babu K, Baer H, Band H, Barnett R, Bergren E, Beringer J, Bernardi G, Bertl W, Bichsel H, Biebel O, Bloch P, Blucher E, Blusk S, Cahn R, Carena M, Caso C, Ceccucci A, Chakraborty D, Chen M, Chivukula R, Cowan G, Dahl O, D'Ambrosio G, Damour T, de Gouvêa A, DeGrand T, Dobrescu B, Drees M, Edwards D, Eidelman S, Elvira V, Erler J, Ezhela V, Feng J, Fetscher W, Fields B, Foster B, Gaisser T, Garren L, Gerber H, Gerbier G, Gherghetta T, Giudice G, Goodman M, Grab C, Gritsan A, Grivaz J, Groom D, Grünewald M, Gurtu A, Gutsche T, Haber H, Hagiwara K, Hagmann C, Hayes K, Hernández-Rey J, Hikasa K, Hinchliffe I, Höcker A, Huston J, Igo-Kemenes P, Jackson J, Johnson K, Junk T, Karlen D, Kayser B, Kirkby D, Klein S, Knowles I, Kolda C, Kowalewski R, Kreitz P, Krusche B, Kuyanov Y, Kwon Y, Lahav O, Langacker P, Liddle A, Ligeti Z, Lin C, Liss T, Littenberg L, Liu J, Lugovsky K, Lugovsky S, Mahlke H, Mangano M, Mannel T, Manohar A, Marciano W, Martin A, Masoni A, Milstead D, Miquel R, Mönig K, Murayama H, Nakamura K, Narain M, Nason P, Navas S, Nevski P, Nir Y, Olive K, Pape L, Patrignani C, Peacock J, Piepke A, Punzi G, Quadt A, Raby S, Raffelt G, Ratcliff B, Renk B, Richardson P, Roesler S, Rolli S, Romaniouk A, Rosenberg L, Rosner J, Sachrajda C, Sakai Y, Sarkar S, Sauli F, Schneider O, Scott D, Seligman W, Shaevitz M, Sjöstrand T, Smith J, Smoot G, Spanier S, Spieler H, Stahl A, Stanev T, Stone S, Sumiyoshi T, Tanabashi M, Terning J, Titov M, Tkachenko N, Törnqvist N, Tovey D, Trilling G, Trippe T, Valencia G, van Bibber K, Vincter M, Vogel P, Ward D, Watari T, Webber B, Weiglein G, Wells J, Whalley M, Wheeler A, Wohl C, Wolfenstein L, Womersley J, Woody C, Workman R, Yamamoto A, Yao W, Zenin O, Zhang J, Zhu R, Zyla P, Harper G, Lugovsky V, Schaffner P (2008) Passage of particles through matter. Physics Letters B 667:267–280
24. Bazilevskaya G, Usoskin I, Flückiger E, Harrison R, Desorgher L, Bütikofer R, Krainev M, Makhmutov V, Stozhkov Y, Svirzhevskaya A, Svirzhevsky N, Kovaltsov G (2008) Cosmic ray induced ion production in the atmosphere. Space Sci Rev 137:149–173
25. Dartnell L, Desorgher L, Ward J, Coates A (2007) Modelling the surface and subsurface martian radiation environment: implications for astrobiology. Geophys Res Lett 34:L02207
26. Dartnell LR, Desorgher L, Ward JM, Coates AJ (2007) Martian sub-surface ionising radiation: biosignatures and geology. Biogeosciences 4:545–558
27. Dartnell LR (2011) Ionizing radiation and life. Astrobiology 11:551–582
28. Nelson GA (2003) Fundamental space radiobiology. Gravitational and Space Biology Bulletin 16:37–44
29. Pavlov A, Blinov A, Konstantinov A (2002) Sterilization of martian surface by cosmic radiation. Planet Space Sci 50:669–673
30. Castenholz R (1988) Culturing methods for cyanobacteria. Methods Enzymol 167:68–93
31. Anderson A, Nordan H, Cain R, Parrish G, Duggan D (1956) Studies on a radio-resistant micrococcus. I. Isolation, morphology, cultural characteristics, and resistance to gamma radiation. Food Technology 10:575–577
32. Dartnell LR, Hunter S, Lovell K, Coates A, Ward J (2010) Low-temperature ionizing radiation resistance of *Deinococcus radiodurans* and Antarctic Dry Valley Bacteria. Astrobiology 10:717–732
33. Dartnell LR, Storrie-Lombardi MC, Mullineaux CW, Ruban AV, Wrigh G, Griffiths AD, Muller J-P, Ward JM (2011) Degradation of cyanobacterial biosignatures by ionizing radiation. Astrobiology 11:997–1016
34. Dartnell LR, Storrie-Lombardi MC, Ward JM (2010) Complete fluorescent fingerprints of extremophilic and photosynthetic microbes. Int J Astrobiol 9:245–257
35. Marshall C, Leuko S, Coyle C, Walter M, Burns B, Neilan B (2007) Carotenoid analysis of halophilic archaea by resonance raman spectroscopy. Astrobiology 7:631–643
36. Edwards H, Moeller R, Jorge Villar S, Horneck G, Stackebrandt E (2006) Raman spectroscopic study of the photoprotection of extremophilic microbes against ultraviolet radiation. Int J Astrobiol 5:313–318
37. Carbonneau M, Melin A, Perromat A, Clerc M (1989) The action of free radicals on *Deinococcus radiodurans* carotenoids. Arch Biochem Biophys 275:244–251
38. Lemee L, Peuchant E, Clerc M, Brunner M, Pfander H (1997) Deinoxanthin: a new carotenoid isolated from *Deinococcus radiodurans*. Tetrahedron 53:919–926
39. Saito T, Ohyama Y, Ide H, Ohta S, Yamamoto O (1998) A carotenoid pigment of the radioresistant bacterium *Deinococcus radiodurans*. Microbios 95:79–90

40. Aasen AJ, Jensen SL (1966) Carotenoids of flexibacteria. 3. The structures of flexixanthin and deoxy-flexixanthin. Acta Chem Scand 20:1970–1988
41. Tao L, Yao H, Kasai H, Misawa N, Cheng Q (2006) A carotenoid synthesis gene cluster from Algoriphagus sp. KK10202C with a novel fusion-type lycopene β-cyclase gene. Mol Genet Genomics 276:79–86
42. Sun Z, Shen S, Wang C, Wang H, Hu Y, Jiao J, Ma T, Tian B, Hua Y (2009) A novel carotenoid 1,2-hydratase (CruF) from two species of the non-photosynthetic bacterium *Deinococcus*. Microbiology 155:2775–2783
43. Tian B, Hua Y (2010) Carotenoid biosynthesis in extremophilic *Deinococcus–Thermus* bacteria. Trends Microbiol 18:512–520
44. Marshall C, Olcott Marshall A (2010) The potential of Raman spectroscopy for the analysis of diagenetically transformed carotenoids. Phil Trans R Soc A 368:3137–3144
45. Makarova K, Aravind L, Wolf Y, Tatusov R, Minton K, Koonin E, Daly M (2001) Genome of the extremely radiation-resistant bacterium *Deinococcus radiodurans* viewed from the perspective of comparative genomics. Microbiol Mol Biol Rev 65:44–79
46. Howell N, Arteaga G, Nakai S, Li-Chan E (1999) Raman spectral analysis in the C–H stretching region of proteins and amino acids for investigation of hydrophobic interactions. J Agric Food Chem 47:924–933
47. Krinsky N (1989) Antioxidant functions of carotenoids. Free Radic Biol Med 7:617–635
48. Edge R, McGarvey D, Truscott T (1997) The carotenoids as antioxidants - a review. Journal of Photochemistry and Photobiology B: Biology, vol 41
49. Armstrong G (1997) Genetics of eubacterial carotenoid biosynthesis: a colorful tale. Annu Rev Microbiol 51:629–659
50. Blasius M, Hübscher U, Sommer S (2008) *Deinococcus radiodurans*: what belongs to the survival kit? Crit Rev Biochem Mol Biol 43:221–238
51. Xu Z, Tian B, Sun Z, Lin J, Hua Y (2007) Identification and functional analysis of a phytoene desaturase gene from the extremely radioresistant bacterium *Deinococcus radiodurans*. Microbiology 153:1642–1652
52. Zhang L, Yang Q, Luo X, Fang C, Zhang Q, Tang Y (2007) Knockout of crtB or crtI gene blocks the carotenoid biosynthetic pathway in *Deinococcus radiodurans* R1 and influences its resistance to oxidative DNA-damaging agents due to change of free radicals scavenging ability. Arch Microbiol 188:411–419
53. de Groot A, Chapon V, Servant P, Christen R, Saux M, Sommer S, Heulin T (2005) *Deinococcus deserti* sp. nov., a gamma-radiation-tolerant bacterium isolated from the Sahara Desert. Int J Syst Evol Microbiol 55:2441–2446
54. Tian B, Xu Z, Sun Z, Lin J, Hua Y (2007) Evaluation of the antioxidant effects of carotenoids from *Deinococcus radiodurans* through targeted mutagenesis, chemiluminescence, and DNA damage analyses. Biochim Biophys Acta 1770:902–911
55. Court R, Sephton M, Parnell J, Gilmour I (2007) Raman spectroscopy of irradiated organic matter. Geochim Cosmochim Acta 71:2547–2568
56. Carr M (1996) Water on Mars. Oxford University Press, Oxford
57. Richmond R, Sridhar R, Daly MJ (1999) Physicochemical survival pattern for the radiophile *Deinococcus radiodurans*: a polyextremophile model for life on Mars. SPIE Conference on Instruments, Methods, and Missions for Astrobiology II 3755:210–222
58. ten Kate I, Garry J, Peeters Z, Foing B, Ehrenfreund P (2006) The effects of martian near surface conditions on the photochemistry of amino acids. Planet Space Sci 54:296–302
59. Gowen RA, Smith A, Fortes AD, Barber S, Brown P, Church P, Collinson G, Coates AJ, Collins G, Crawford IA, Dehant V, Chela-Flores J, Griffiths AD, Grindrod PM, Gurvits LI, Hagermann A, Hussmann H, Jaumann R, Jones AP, Joy KH, Karatekin O, Miljkovic K, Palomba E, Pike WT, Prieto-Ballesteros O, Raulin F, Sephton MA, Sheridan S, Sims M, Storrie-Lombardi MC, Ambrosi R, Fielding J, Fraser G, Gao Y, Jones GH, Kargl G, Karl WJ, Macagnano A, Mukherjee A, Muller JP, Phipps A, Pullan D, Richter L, Sohl F, Snape J, Sykes J, Wells N (2011) Penetrators for in situ subsurface investigations of Europa. Adv Space Res 48:725–742